NJC

New Journal of Chemistry

A journal for new directions in chemistry

Accepted Manuscript

This article can be cited before page numbers have been issued, to do this please use: D. Madhav, M. Malankowska and J. Coronas, *New J. Chem.*, 2020, DOI: 10.1039/D0NJ04402D.

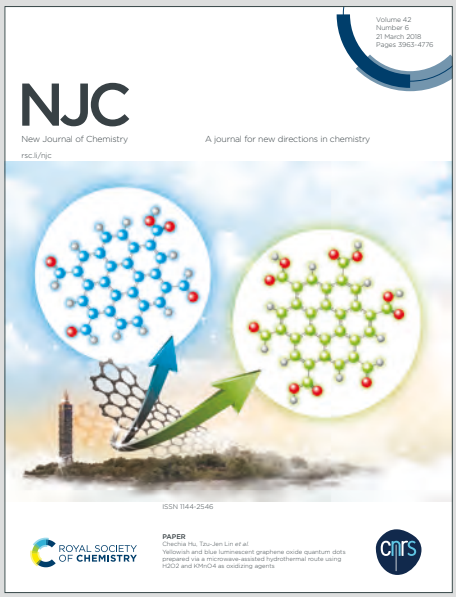

This is an Accepted Manuscript, which has been through the Royal Society of Chemistry peer review process and has been accepted for publication.

Accepted Manuscripts are published online shortly after acceptance, before technical editing, formatting and proof reading. Using this free service, authors can make their results available to the community, in citable form, before we publish the edited article. We will replace this Accepted Manuscript with the edited and formatted Advance Article as soon as it is available.

You can find more information about Accepted Manuscripts in the Information for Authors.

Please note that technical editing may introduce minor changes to the text and/or graphics, which may alter content. The journal's standard Terms & Conditions and the Ethical guidelines still apply. In no event shall the Royal Society of Chemistry be held responsible for any errors or omissions in this Accepted Manuscript or any consequences arising from the use of any information it contains.

ROYAL SOCIETY OF CHEMISTRY

rsc.li/njc

Synthesis of nanoparticles of zeolitic imidazolate framework ZIF-94 using inorganic deprotonators

Dharmjeet Madhav[1,2], Magdalena Malankowska[1,2,*], Joaquín Coronas[1,2,*]

[1]Instituto de Nanociencia y Materiales de Aragón (INMA), Universidad de Zaragoza-CSIC, 50018 Zaragoza, Spain.

[2]Chemical and Environmental Engineering Department, Universidad de Zaragoza, 50018 Zaragoza, Spain.

* Corresponding authors' email: magnal@unizar.es, coronas@unizar.es

Abstract

A novel synthesis process of ZIF-94 (also known as SIM-1) is developed for particle size tuning, using either NaOH or NH_4OH as deprotonators. ZIF-94 stem from MOFs and have several advantages over traditional porous materials, dealing with their chemistry, structure and with their applications as catalysts, adsorbents, biocides and membrane materials. The existing synthesis process of ZIF-94 at scale-up level produces particles of approximately 250 nm in size; having even smaller size is expected to give even better gas separation performance and catalytic activity. In this study, it was found that NaOH gives ZIF-94 particles with well-defined crystal structure while in the case of NH_4OH, particles agglomerated to produce random shaped bigger particles. The optimum base to metal ratio was found to be 2:1 (NaOH:Zn), which gives a compromise between particle size and surface area, such amount of base loading gives a SEM average particle size of 114 ± 3 nm with BET specific surface area of 254 ± 4 m^2/g. Furthermore, the synthesized nanoparticles underwent a thorough characterization by XRD, TGA, N_2 adsorption and electronic microscopy revealing the lowest SEM average particle size of 84 ± 3 nm.

Keywords: MOF, ZIF-94, SIM-1, Particle size tuning, Nanoparticle synthesis

View Article Online
DOI: 10.1039/D0NJ04402D

1. Introduction

Metal organic frameworks (MOFs) or coordination polymers are crystalline porous organic-inorganic hybrid materials. Since their appearance in 1980s, they have attracted great attention among researchers due to their fascinating properties and potential applications.[1] Zeolite imidazolate frameworks (ZIFs) are an important subclass of MOFs comprised of tetrahedral metal ions linked by imidazolate moieties.[2] ZIFs have several advantages over traditional porous materials, such as ultramicroporosity, flexible structure, selective gas uptake, higher chemical stability, adjustable properties, and easy functionalization.[3] Thanks to these outstanding features, ZIFs have been explored for potential applications in gas separation /storage,[4,5] liquid separation,[6] water purification,[7] catalysis and adsorption,[8] sensors,[9] drug delivery and other medical applications.[10,11] Iron-doped ZIF-8 catalyst gives a 96.6 % yield of cyclic carbonate synthesis from CO_2 cycloaddition.[12] Dong and Zheng[13] have constructed a novel H_2O_2 sensor using cobalt-based ZIF, ZIF-67. Sun *et al.*[10] reported a ZIF based pH-responsive drug delivery system for effective antitumor therapy. Hollow fiber membranes incorporated with ZIF-8, for water purification, showed better performance in small molecule separations. They reject up to 99.5% of small molecules with molecular weight 320 to 800 Da at high permeance of up to 50 L m^{-2} h^{-1} bar^{-1}.[7] ZIFs are indeed in focus for their application as fillers in MMMs, and it was demonstrated to have great potential for CO_2 capture and separation. In a recent study, lithium-modified ZIF-91 showed CO_2 uptake up to 10 mmol·g^{-1}.[14] ZIF-8, when used as filler in MMMs, increases the permeability of CO_2 through membranes without affecting much the selectivity over other gases.[15–17] Similarly, a highly permeable and selective membrane of ZIF-95 has been developed for H_2/CO_2 separation.[18]

A less explored ZIF, ZIF-94, also called SIM-1 (substituted imidazolate material-1), has shown to have promising properties to be used as filler in MMMs for gas separation,[19,20] continuous membrane,[20,21] adsorbent for biomass-derived polyols,[22] catalyst,[23] biocidal material,[24,25] and CO_2 adsorbent.[26] As ZIF-8, ZIF-94 also crystallizes in the sod topology constructed by Zn atoms and 4-methyl-5-imidazole-carboxaldehyde links (Fig. 1).[27]

View Article Online
DOI: 10.1039/D0NJ04402D

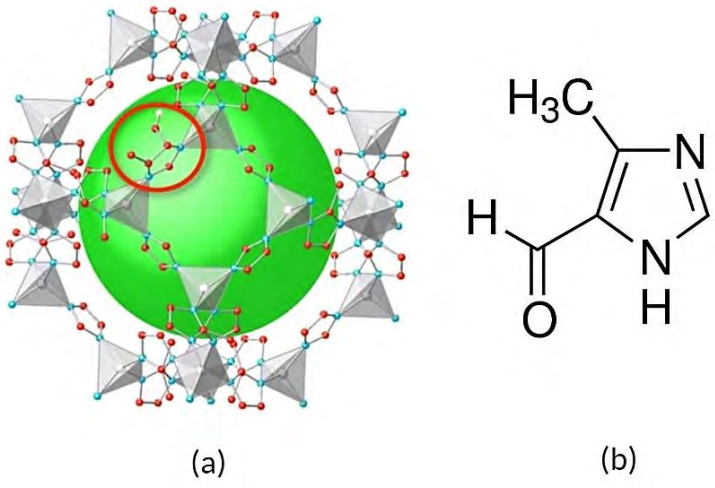

Fig. 1. *ZIF-94 framework with the linker represented in red circle, where blue, red and white dots represent nitrogen, carbon and oxygen atoms respectively (a), ZIF-94 linker 4-methyl-5imidazolecarboxaldehyde (b). Adapted with permission from [27].*

ZIF-94 is characterized by high CO_2 uptake of 2.4 mmol g^{-1} even at low pressure of 1 bar which is higher in comparison to other ZIFs i.e. ZIF-93 (1.7 mmol g^{-1}), ZIF-7 (1.6 mmol g^{-1}) and ZIF-11 (0.8 mmol g^{-1}).[19] The higher CO_2 uptake is due to the smaller pore diameter of ZIF-94 compared to other ZIFs as well as due to the specific interaction with its aldehyde group. It is expected that the smaller particles of ZIF-94 would further improve the CO_2 uptake.[26] Particle size of catalyst highly influences the catalytic effect; the smaller particles show better catalytic activity.[28,29] Furthermore, smaller particles of ZIF-8 in polysulfone (PSf) membrane result in higher CO_2/CH_4 selectivity.[30] However, the particle size of ZIF-94 is yet to be optimized. Several attempts to modify the properties such as pore size, particle size and particle size distributions have been made by using various solvents and modifying metal to ligand ratio at different reaction conditions as well as by using post-synthetic modifications.[19,21,22,27,31,32] The smallest average particle size of ZIF-94 synthesised at scale-up level till date is ca. 250 nm.[31]

Here a novel way of synthesising ZIF-94 nanoparticles with an average particle size below 100 nm, is reported using inorganic deprotonators NaOH and NH_4OH. Smaller particles of ZIF-94 synthesised through this procedure could improve its catalytic activity, CO_2 uptake and polyol adsorption.

2. Experimental Section

2.1. Materials

Zinc acetate dihydrate ($Zn(CH_3COO)_2 \cdot 2H_2O$), 98% and 4-methyl-5-imidazolecarboxaldehyde ($C_5H_6N_2O$), 99% were purchased from Acros Organics. Tetrahydrofuran (THF), anhydrous,

99.9% and ammonium hydroxide solution (NH_4OH), 28-30% NH_3 base were obtained from Sigma-Aldrich. Methanol and sodium hydroxide (NaOH), pellets were supplied by Scharlab S.L., Spain. All the chemicals were used as obtained from the manufacturer without any further purification.

2.2. ZIF-94 synthesis

First, ZIF-94 synthesis by Johnson *et al.*[31] was reproduced and termed as the original method. Briefly, 528 mg (2.4 mmol) of zinc acetate dihydrate was dissolved in 2 mL of methanol. In a separate vial, 528 mg (4.8 mmol) of 4-methyl-5-imidazolecarboxaldehyde was dissolved in 5 mL THF. After stirring each for 10 min separately, metal salt solution in methanol was added into the ligand suspension in THF under vigorous mixing. The final reaction mixture was kept under continuous stirring for 16 h at room temperature (RT). Finally, the product was collected by centrifugation at 11000 rpm for 10 min and washed three times with methanol through the same centrifugation procedure. Ultrasonication was used during washing for proper mixing of the product into methanol. The sample obtained after washing was mixed properly in methanol, sonicated and dried at RT under a fume hood for 48 h.

2.3. ZIF-94 synthesis – modification of the original method

It has been found that the basic medium of synthesis solution promotes deprotonation of linker and the pH affects the nucleation, crystallization and growth of ZIFs.[33,34] Therefore, the effect of two different bases was investigated to elucidate their effect on the particle size of ZIF-94: NaOH and NH_4OH. The bases were added at various ratios keeping the metal:ligand ratio constant (Table 1).

Table 1. *Original method modifications with constant metal to ligand ($Zn(CH_3COO)_2{\cdot}2H_2O$:$C_5H_6N_2O$) molar ratio of 1:2 to adjust the ZIF-94 particles size.*

Sample	Base	Base:Zn molar ratio	Amount of base (mg)
1	NaOH	0.5:1	48
2	NaOH	1:1	96
3	NaOH	2:1	192
4	NaOH	3:1	289
5	NH_4OH	1:1	84

For the NaOH procedure, the same amount and composition of the metal salt solution and ligand suspension were prepared as stated above. NaOH pellets were firstly crushed to obtain powdered NaOH for better mixing in the synthesis suspension. Next, 48 mg (1.2 mmol), 96 mg (2.4 mmol), 192 mg (4.8 mmol) and 289 mg (7.2 mmol) of solid NaOH was added to the zinc

View Article Online
DOI: 10.1039/D0NJ04402D

acetate solution in order to obtain 0.5:1, 1:1, 2:1 and 3:1 base to the metal molar ratio in the final reaction mixture, respectively (Table 1). Zinc acetate solution containing NaOH was stirred for 10 min and then it was added into the pre-stirred ligand suspension. The final mixture was stirred at RT for 16 h. The product was collected, washed with methanol and dried at room temperature as described in the original method, where THF/methanol solution was used as a solvent without any base deprotonators.[31]

In case of the NH_4OH procedure, 146 mg of 57.7 wt% aqueous NH_4OH was added to the zinc acetate solution. The effective amount of NH_4OH present in the water solution was 84 mg (2.4 mmol) resulting in 1:1 base to metal ratio in the final reaction mixture. The rest of the steps were the same as it was described in the case of NaOH. The experimental scheme of synthesis process can be found in the supplementary information (Fig. S1).

The amount of base for both cases was calculated using a general equation (equation 1):

$$M_{Base} = n_{Zn(CH_3COO)\cdot H_2O} \cdot r \cdot M_W \quad (1)$$

Where M_{Base} is the amount of base that had to be added to the synthesis (g), $n_{Zn(CH_3COO)\cdot H_2O}$ is the number of moles of zinc acetate dihydrate (mol), r is the required ratio of a base (-), and M_w is the molecular weight of the base (g/mol).

2.4. ZIF-94 characterization

2.4.1. Powder X-ray diffraction (PXRD)

Powder X-ray diffraction data were collected using Panalytical Empyrean equipment with CuK_α radiation (λ = 0.154 nm), over the range of 5º - 40º at a scan rate of 0.03º s^{-1}, to examine the *d*-spacing of the nanoparticles. Obtained data were compared to the simulated data available online.[35,36]

2.4.2. Thermogravimetric analysis (TGA)

TGA was carried out using a Mettler Toledo TGA/STDA 851e. Small amount of the sample (approx. 5 mg) placed in 70 µL alumina pans was heated under airflow (40 mL min^{-1}) from 35 to 700 ºC at a heating rate of 10 ºC min^{-1}. Normalised weight versus temperature curve was plotted.

View Article Online
DOI: 10.1039/D0NJ04402D

2.4.3. N_2 adsorption-desorption and BET surface area

N_2 adsorption-desorption isotherms were obtained using Micrometrics Tristar 3000 at 77 K. Before these measurements, ZIF-94 samples were degassed for 8 h under vacuum at 200 °C using a heating rate of 10 ºC min^{-1}. Nitrogen adsorption-desorption was performed to obtain the quantity adsorbed and desorbed versus relative pressure. The surface area was calculated using the Brunauer-Emmett-Teller (BET) method. Collected data were analysed to obtain BET surface area and N_2 adsorption-desorption isotherm.

2.4.4. Scanning Electron Microscopy (SEM)

The morphology of ZIF-94 nanoparticles was examined by scanning electron microscopy (SEM) with backscattered electron mode using an Inspect F50 model scanning microscope (FEI), operated at 10 kV. The image at 50,000 magnification from three spots in each sample was analysed with ImageJ software and particle size distribution was obtained.

2.4.5. Transmission Electron Microscopy (TEM)

Samples were analysed through transmission electron microscopy (TEM) to examine the possibility of aggregation. The sample suspension in methanol was placed onto a carbon-coated copper 300 mesh TEM grid and observed under FEI Tecnai T20 transmission electron microscope operated at 200 kV.

3. Results and Discussion

Figure 2 shows the schematic representation of the modifications carried out in the original method to obtain different products to be characterized by the various techniques mentioned in section 2.4.

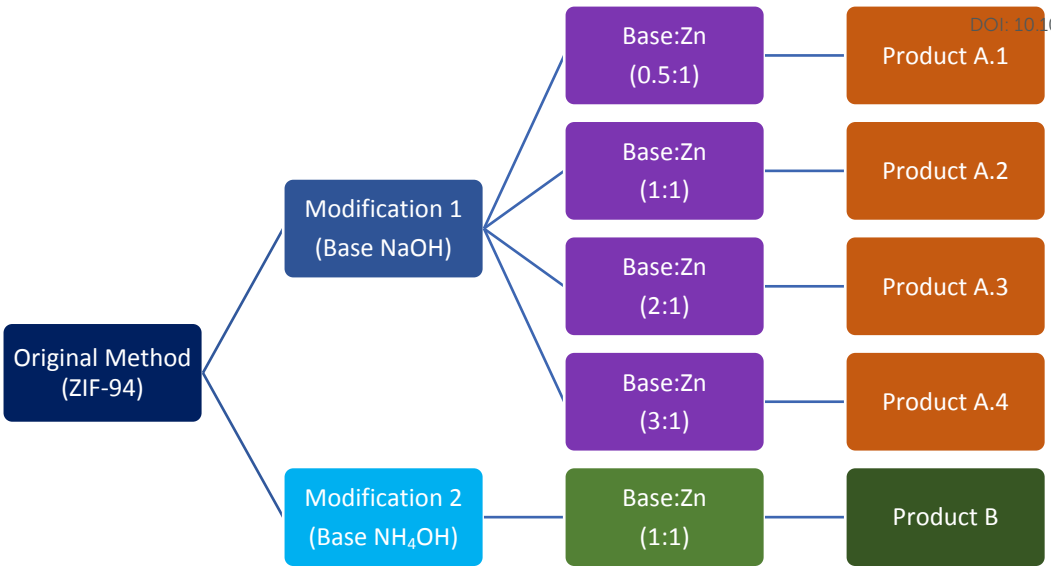

Fig. 2. *Schematic representation of modification in the original method to obtain different products*

3.1. Original method

X-ray diffraction pattern determines the crystallinity of the product and the absence of any additional crystal phases. Figure 3A shows that the XRD pattern of product synthesised via the original method corresponds to the simulated data.[35,36] Peak positions and relative intensities match well with single crystal data corresponding to ZIF-94. Miller indices (hkl) corresponding to each peak have been calculated, and this confirms that the sample has cubic phase structure and matches well with the values reported earlier for ZIF-8 (complete calculation process has been provided in the supplementary information, Table S1).[37]

Thermogravimetric analysis of all the samples was performed in the temperature range of 35 °C to 700 °C to evaluate the thermal stability of prepared nanomaterials. TGA curve shows that pure, activated material was obtained (no significant weight loss in the ca. 200-300 ºC range suggesting the absence of trapped ligand). Nevertheless, the particles contained some residuals of the solvent, since the first decrease in the curve (up to approximately 85 ºC) corresponds to the solvent evaporation. There is a rapid weight loss after 300 °C which is due to the degradation of the sample and it confirms that thermal stability of the particles is up to 300 °C (Fig. 3B).

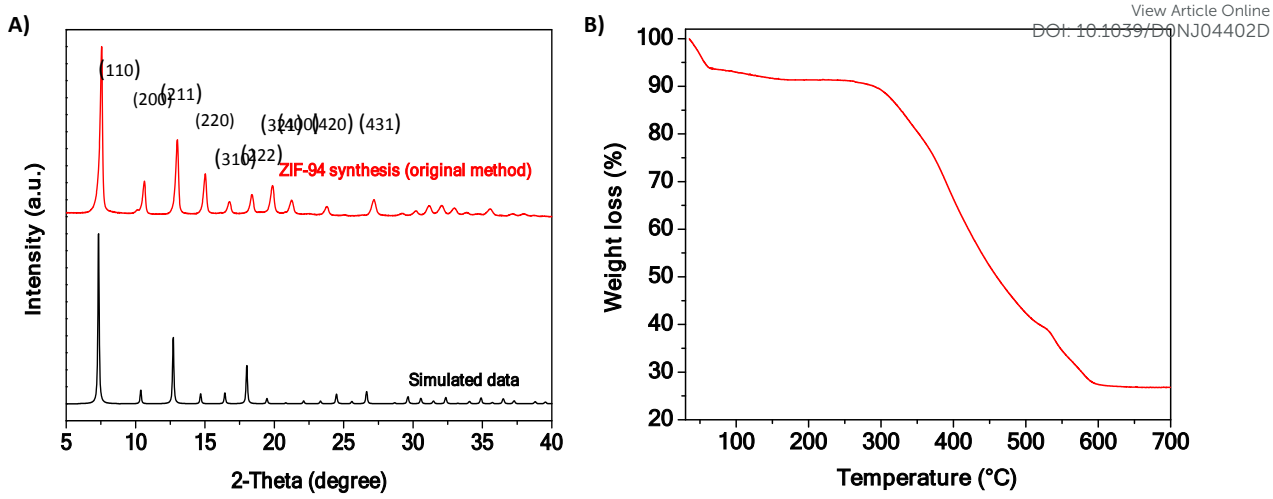

Fig. 3. *XRD pattern of particle prepared through the original method compared with simulated data available online (A); TGA curve of particles prepared through the original method (B)*

N_2 adsorption-desorption and BET theory are the techniques that are used to measure the quantity of an adsorbed gas, the nanoparticle pore volume and surface area. Even though the XRD pattern of ZIF-94 is the same as that of ZIF-8, the BET area distinguishes the two materials very well. In several reports, the surface area of ZIF-8 was found to be between 1300 and 1810 m^2/g,[38,39] while Jin *et al.*[22] reported the surface area of 363 m^2/g for ZIF-94. BET surface area of the particles synthesised through the original method was found to be 326 ± 10 m^2/g which is comparable to the reported data.[22] N_2 adsorption isotherm (Fig. 4) is concave towards P/P° axis with steep uptake at the very low value of P/P°. The quantity adsorbed approaches to maximum when P/P° reaches towards its maximum. Similar isotherm was obtained by Johnson *et al.*[31] for ZIF-94 and it is the typical type I isotherm given by microporous solid.[40]

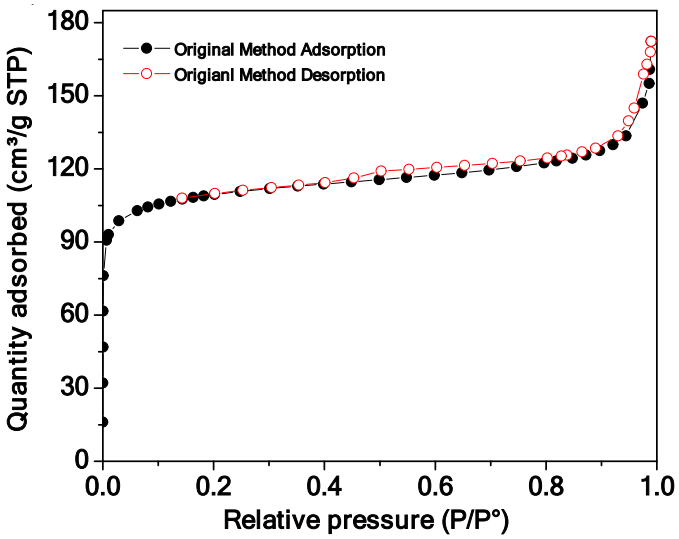

Fig. 4. *N_2 adsorption-desorption isotherm of ZIF-94 synthesised by the original method*

View Article Online
DOI: 10.1039/D0NJ04402D

SEM image (Fig. 5A) shows that ZIF-94 nanoparticles obtained in the original method have a well-defined crystal structure and that they are well separated with variation in size. Particle size distribution (Fig. 5B) obtained from measuring around 40 particles from three such images taken at three different spots of the sample indicates that the particle size is between 100 to 350 nm. The majority of the particles possess a size between 200 to 250 nm making the average particle size of 212 ± 7 nm.

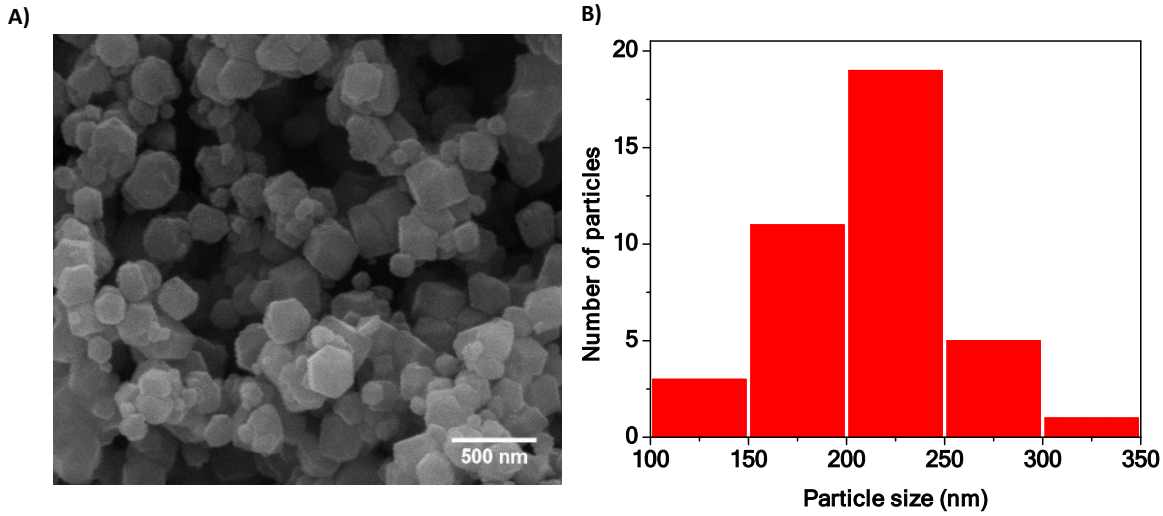

Fig. 5. *SEM image of original method particles (A); particle size distribution obtained from three SEM images taken from different spots in the sample (B)*

3.2. Modified ZIF-94 synthesis

Five samples of ZIF-94 particles were synthesised after the modification of the original method. Products A.1-A.4 and product B were obtained by adding different amount of two bases NaOH and NH_4OH, respectively (see Fig. 2 for a scheme). All the samples prepared through a modified method possess XRD patterns that correspond to ZIF-94, which in turn correspond to that of ZIF-8 since both materials share the same sod type structure.[41] XRD patterns of product A.2-A.3 (Fig. 6A) and B (Fig. 7A) have a broader peak. Scherrer equation[42] suggests that this broad peak could indicate the smaller particle size in these samples. In fact, the calculation with this equation (at 2-theta value of ca. 7.5º) revealed particle sizes in the range of 30-38 nm (30-38 nm for A.1-A.4 and 21 nm for B), not seen in the SEM images suggesting important particle agglomeration. The size of the particles calculated through this method (Table 2) is somewhat in agreement with the particle size calculated from SEM images i.e. particle size decreases for samples prepared using NaOH and NH_4OH. The complete calculation procedure, equation used and average particle size using all the peaks can be found in the supplementary information (Table S2).

Table 2. *The particle sizes of all the samples calculated using Scherrer equation, at the values of 2-theta ca. 7.5° and K equals to 0.94*

Sample	Peak position (2theta)	FWHM	Crystal Size (nm) (Kλ/β cos θ)
Original Method	7.48	0.23	36
Product A.1	7.47	0.25	33
Product A.2	7.47	0.28	30
Product A.3	7.51	0.25	33
Product A.4	7.46	0.22	38
Product B	7.60	0.39	21

TGA curves of products A.1-A.4 (Fig. 6B) and product B (Fig. 7B) show that the thermal decomposition of all the samples occurs at around 300 °C which is in agreement with the ZIF-94 particles obtained by the original method. There is a maximum of 10 % weight loss around 85 °C due to THF and methanol removal. All the solvent trapped inside the sample did not evaporate even after 48 h of drying at RT which suggests that a more rigorous drying method like heating the sample below the thermal decomposition in a vacuum oven could be used.

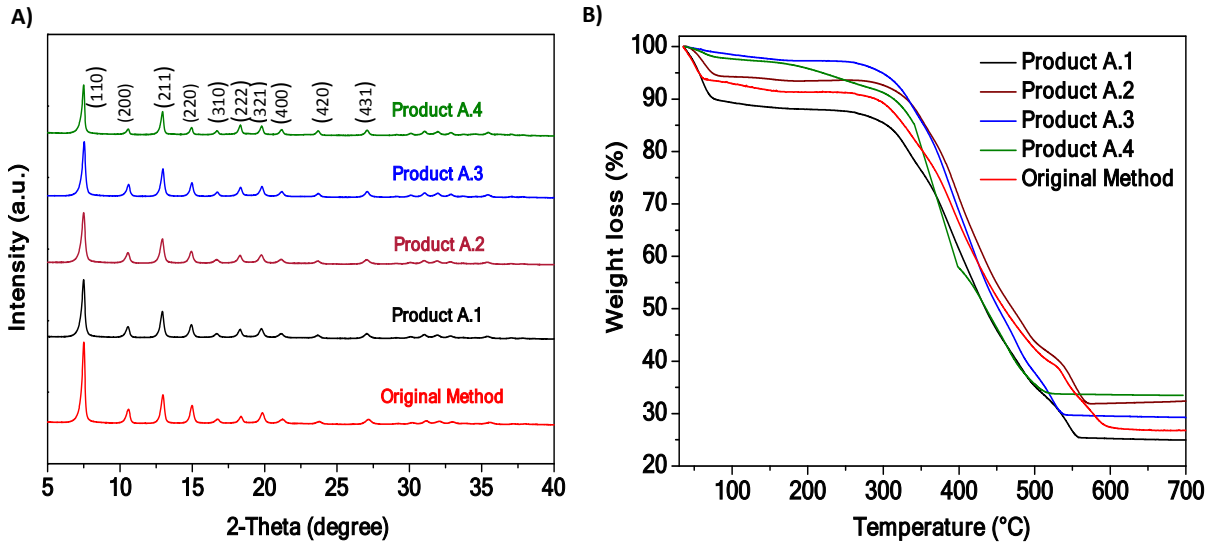

Fig. 6. *XRD patterns of samples produced through modified original method using base NaOH compared with original method samples (A); TGA curve of those samples in comparison with original method sample (B)*

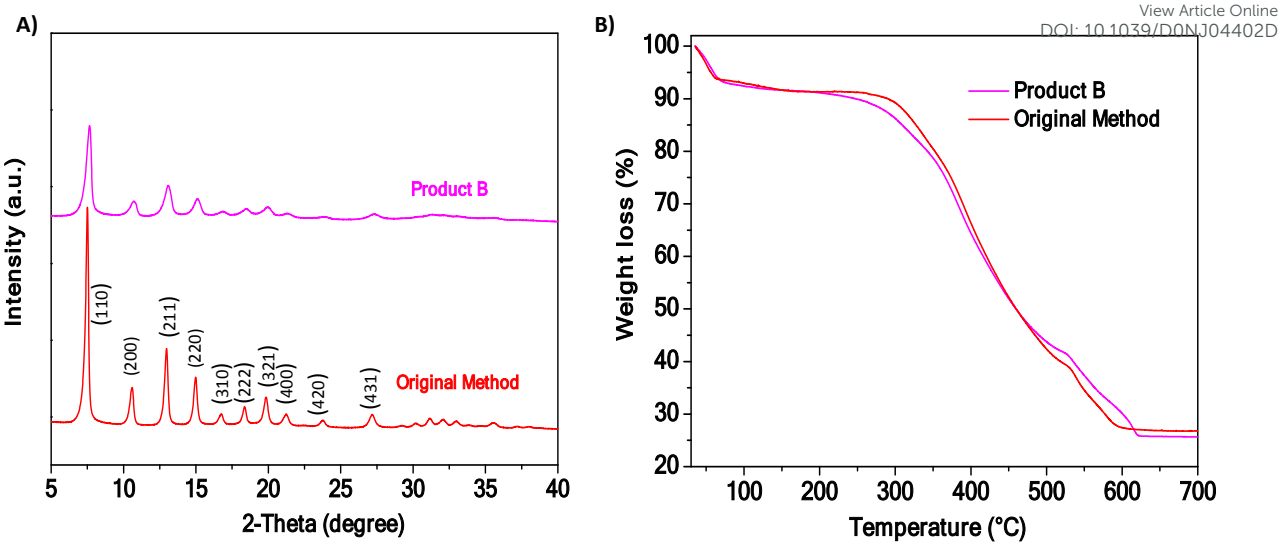

Fig. 7. *XRD patterns of sample produced through modified original method using base NH_4OH compared with original method samples (A); TGA curve in comparison with original method sample (B)*

BET surface area confirms that all the samples synthesised through the modified method are pure phase ZIF-94. The surface area of products A.1-A.4 and B is found to be 119 ± 2, 209 ± 3, 254 ± 4, 135 ± 1 and 277 ± 5 m^2/g, respectively (Fig. 8A-9A). However, all products exhibit smaller BET surface area compared to the original method, which can be due to a less crystalline structure (broad XRD peaks) as the particle size decreased. Similar phenomena has been observed earlier for ZIF-8 - BET surface area becomes smaller as particle size decreases.[43] Moreover, TGA results suggest that the degasification treatment at 200 ºC (before N_2 adsorption) should be enough for trapped solvents and ligand removal. XRD pattern and TGA curve of the activated sample (200 ºC for 8 h) further confirm the absence of any trapped ligand or guest molecule in the samples (Fig. S4, supplementary information). Adsorption isotherms of products A.1-A.4 (Fig. 8B) and product B (Fig. 9B) are comparable to the isotherm of original ZIF-94 (Fig. 4) indicating type I isotherm given by microporous solids.[40] A slight hysteresis is observed in all isotherms that may be due to capillary condensation in the spaces in between the nanoparticles.[40] Furthermore, pore volumes were calculated from nitrogen adsorption data and it was found that the values decreased from 0.23 cm^3/g for original method samples to 0.16 cm^3/g for product A.4 (find pore volume and pore size of all the samples in the supplementary information, Table S3). The diameter of ZIF-94 cavities is 0.75 nm,[41] what suggests a pore limiting dimension of ca. 0.3 nm, something below the 0.34 nm of ZIF-8 with the same sod structure and 1.14 nm cavities.[39]

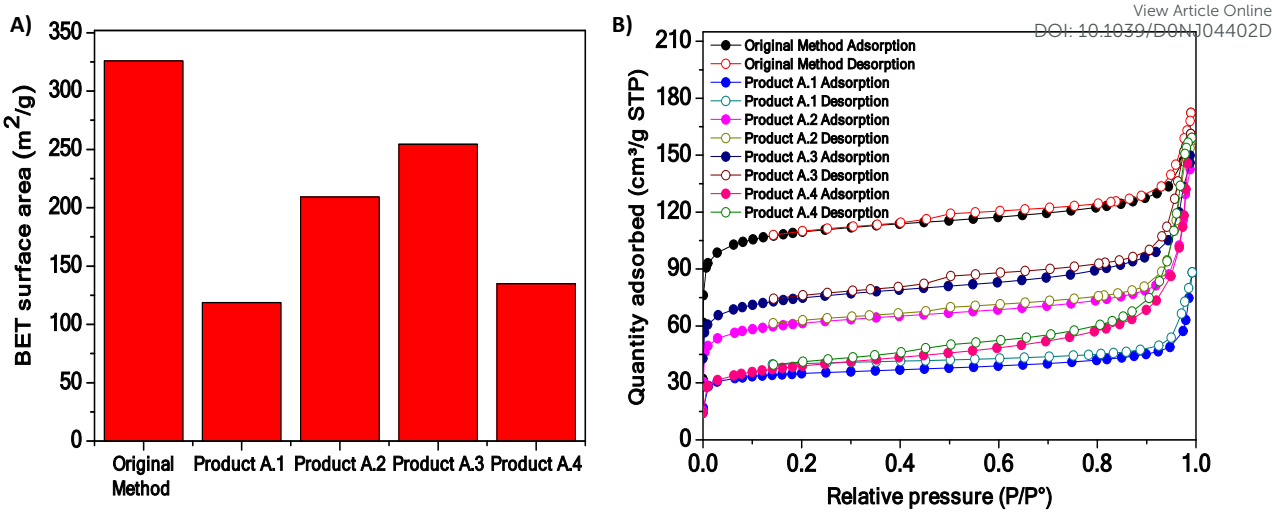

Fig. 8. *BET surface area comparison of all the samples produced through modified original method using base NaOH with original method samples (A); N2 adsorption isotherm of those samples compared with original method (B)*

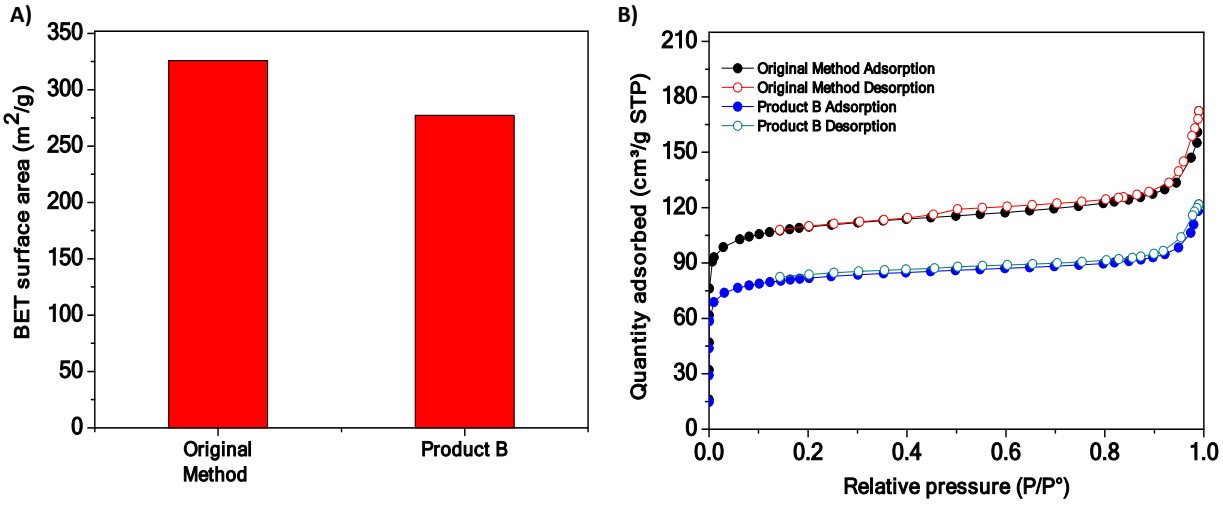

Fig. 9. *BET surface area comparison of sample produced through modified original method using base NH_4OH with original method samples (A); N2 adsorption isotherm of product B compared with original method (B)*

SEM observation, particle size distribution and average particle size are crucial factors in this study. Our objective was to reduce the particle size of ZIF-94 in comparison to the widely used synthesis procedures. From SEM images (Fig. 10 A-E), the particle size distribution (Fig. 11) and average particle size were obtained. Particle size found to be gradually decreasing with an increased amount of base addition. The average particle size of products A.1- A.4 found to be 142 ± 6, 110 ± 5, 114 ± 3, and 84 ± 3 nm, respectively. Product B, in which NH_4OH was added, does not acquire the well-defined shape of ZIF-94 (Fig. 10 E) the average particle size found to be 636 ± 51 nm with most particles in the size range of 500-700 nm (Fig. 11). Even after having broad XRD peaks which suggest smaller particles, SEM image shows bigger structures. This is due to the agglomeration of small particles probably occurred because since NH_4OH is

not as strong base as NaOH it could not completely deprotonate the linkers resulting in slow crystallization and agglomeration. While NaOH, being a strong base, completely deprotonates imidazole linker leading to increased nucleation rate and rapid crystallization resulting in less agglomerated ZIF-94. The proposed mechanism of the synthesis using NaOH is shown in Fig. 12. OH^- from the base would deprotonate the imidazole linker and facilitate coordination bonding with Zn^{2+}. On the other hand, in the case of synthesis using NH_4OH, the mechanism is similar considering OH^- deprotonating the imidazole linker; however in this case, extra water (besides that coming from the ligand deprotonation, one water molecule per deprotonated ligand molecule, and that consubstantial to the Zn acetate, two water molecules per Zn atom) was present in the reaction mixture which has been reported to facilitate the hydrolysis of the linker and eventually helping in coordination with Zn^{2+} in the synthesis of a similar ZIF, ZIF-8.[44] At the same time due to the presence of water in the reagent, there is a possibility of hydrolysis of ZIF-94, which strongly depends on the amount of water present in the system. Drastic change in XRD pattern of ZIF (ZIF-8) has been reported after hydrolysis,[45] while the XRD pattern of product B (synthesized with NH_4OH) is identical to that of the product corresponding to the original method. This suggests that the extent of hydrolysis if occurred was not enough to reverse the synthesis and to show any significant impact. However, the effect of the presence of water on the crystallinity of the product cannot be neglected and that could also be the reason of agglomeration of ZIF particles in the product B leading to randomly shaped bigger particles. Interestingly, for product B, TEM observation revealed an average particle size of 369 ± 17 nm suggesting that the particles are strongly agglomerated from much smaller MOF nanoparticles (those illustrated by the Scherrer calculation) (see Table 3 for the summary of the characteristic of all products synthesised).

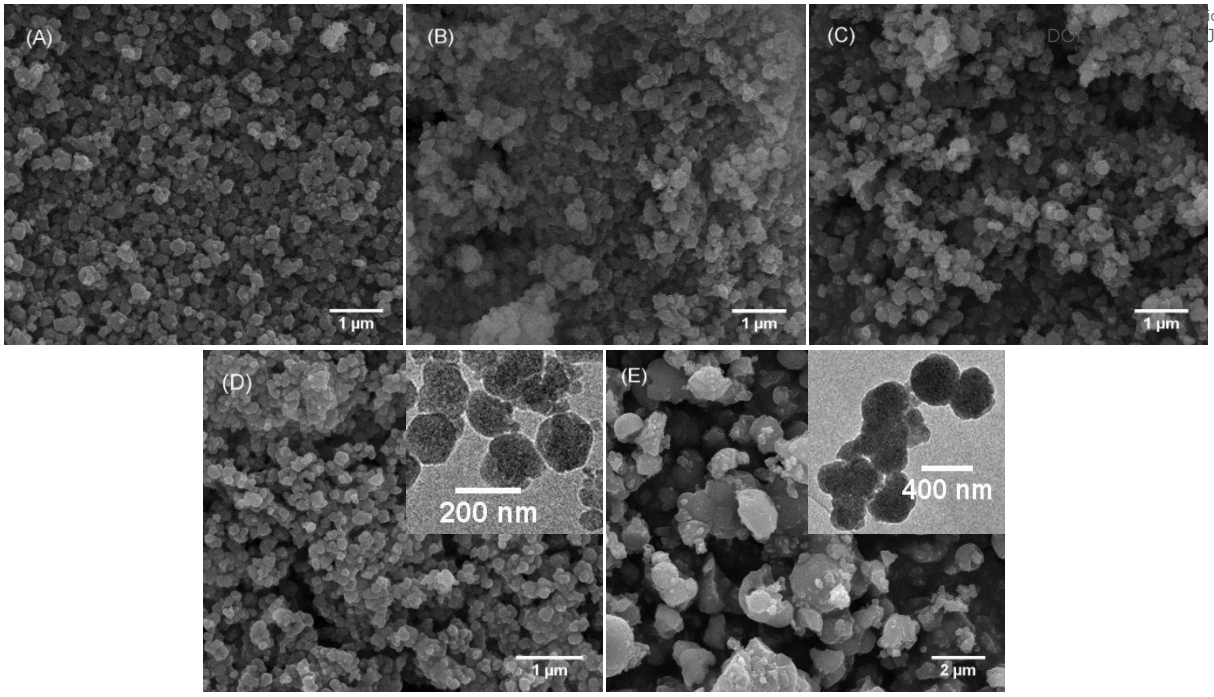

Fig. 10. *SEM images of product A.1 (A), product A.2 (B), product A.3 (C), product A.4 (D), product B (E) and TEM images of product A.4 and B in the inset (complete TEM images can be found in supplementary information).*

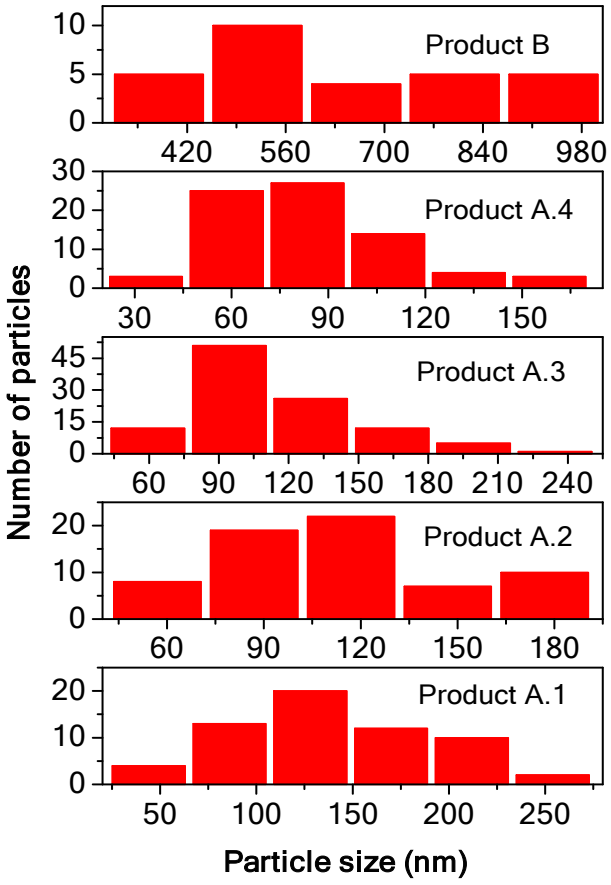

Fig. 11. *Particle size distribution of product A.1-A.4 to B (from bottom to top)*

View Article Online
DOI: 10.1039/D0NJ04402D

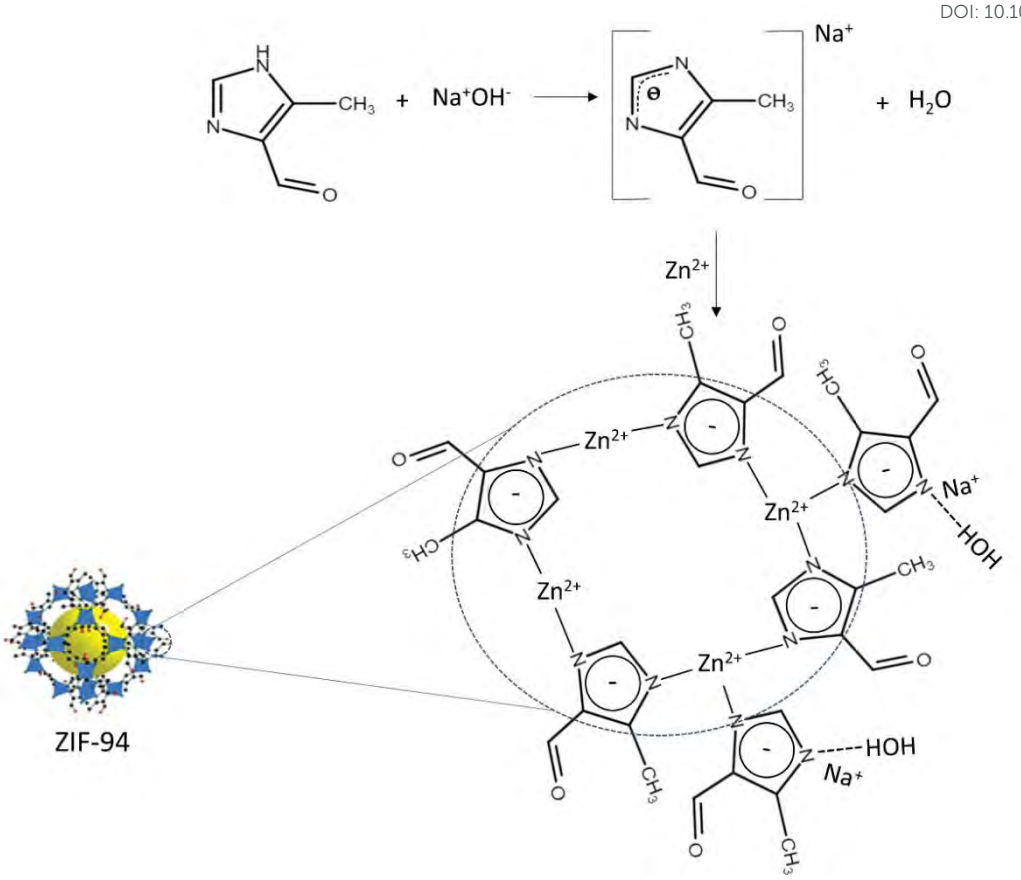

Fig. 12. *Proposed mechanism of ZIF-94 synthesis using NaOH as deprotonator*

Table 3. *Summary of characteristics of original ZIF-94 and products obtained through different modifications of original method*

Sample	Characteristics		Comparison to the literature		
	Avg. particle size (nm)	BET area (m^2/g)	Avg. particle size	BET area (m^2/g)	Ref.
Original ZIF-94	212 ± 7	326 ± 10	340 nm	424	19
Product A.1	142 ± 6	119 ± 2	800 nm	591	20
Product A.2	110 ± 5	209 ± 3	4 µm	363	22
Product A.3	114 ± 3	254 ± 4	275 nm	415	31
Product A.4	84 ± 3	135 ± 1	3 µm	602	32
Product B	636 ± 51	277 ± 5	472 nm	415	27

View Article Online
DOI: 10.1039/D0NJ04402D

4. Conclusions

ZIF-94 is an emerging material with many potential applications. The target of this work was to synthesise ZIF-94 at room temperature and to decrease the particle size by using two bases (NaOH or NH_4OH) that will work as deprotonators.

The particle size of ZIF-94 was successfully reduced down to about 84 nm, compared to approximately 250 nm given by the commonly used methods. Synthesis of ZIF-94 with NaOH as a deprotonator resulted in particles with well-defined crystal structure, as inferred from XRD characterization. On the other hand, in case of using NH_4OH as a base, particles agglomerated to produce random shaped bigger structures. This is because NaOH, being significantly stronger base than NH_4OH, shows a severe effect on the nucleation rate and induces rapid crystallization during synthesis. The higher amount NaOH with respect to metal gradually reduced the particle size but at the cost of sacrificing the BET specific surface area, resulting in a conclusion that, in both cases, very small and very big amount of NaOH additions have disadvantageous effects. Base addition at the ratio 2:1 (NaOH:Zn) gives a compromise between particle size (average particle size of 114 ± 3 nm) and surface area (254 ± 4 m^2/g). Therefore, smaller ZIF-94 particles synthesised at these conditions constitute a breakthrough and needed to be further investigated for their catalytic activity, adsorption efficiency, biocidal effect and most importantly as the fillers in MMMs.

Conflicts of interest

The authors declare to have no conflict of interest.

Acknowledgements

Financial support from the Spanish Project MAT2016-77290-R (AEI/ FEDER, UE) MINECO, the Aragón Government (T43-17R) and the ESF are gratefully acknowledged. D. M. thanks the European Commission - Education, Audiovisual and Culture Executive Agency (EACEA) for Erasmus Mundus scholarship under the program: Erasmus Mundus Master in Membrane Engineering for a sustainable world (EM3E-4SW), he extends his gratitude to his colleague Sara Chergaoui for the fruitful discussions. All the microscopy work was done in the Laboratorio de Microscopías Avanzadas at the Instituto de Nanociencia de Aragón (LMA-

INA). The authors acknowledge the LMA-INA for offering access to their instruments and expertise.

References

1 D. Bazer-Bachi, L. Assié, V. Lecocq, B. Harbuzaru and V. Falk, *Powder Technology*, 2014, **255**, 52–59.
2 B. Wang, A. P. Côté, H. Furukawa, M. O'Keeffe and O. M. Yaghi, *Nature*, 2008, **453**, 207–211.
3 B. Chen, Z. Yang, Y. Zhu and Y. Xia, *J. Mater. Chem. A*, 2014, **2**, 16811–16831.
4 C. Duan, H. Zhang, F. Li, J. Xiao, S. Luo and H. Xi, *Soft Matter*, 2018, **14**, 9589–9598.
5 J. Hou, Y. Wei, S. Zhou, Y. Wang and H. Wang, *Chemical Engineering Science*, 2018, **182**, 180–188.
6 S. Basu, M. Maes, A. Cano-Odena, L. Alaerts, D. E. De Vos and I. F. J. Vankelecom, *Journal of Membrane Science*, 2009, **344**, 190–198.
7 W. Wu, M. Jia, J. Su, Z. Li and W. Li, *AIChE J*, , DOI:10.1002/aic.16238.
8 Y. Guan, J. Shi, M. Xia, J. Zhang, Z. Pang, A. Marchetti, X. Wang, J. Cai and X. Kong, *Applied Surface Science*, 2017, **423**, 349–353.
9 G. Ren, Z. Li, W. Yang, M. Faheem, J. Xing, X. Zou, Q. Pan, G. Zhu and Y. Du, *Sensors and Actuators B: Chemical*, 2019, **284**, 421–427.
10 Q. Sun, H. Bi, Z. Wang, C. Li, X. Wang, J. Xu, H. Zhu, R. Zhao, F. He, S. Gai and P. Yang, *Biomaterials*, 2019, **223**, 119473.
11 A. Mazloom-Jalali, Z. Shariatinia, I. A. Tamai, S.-R. Pakzad and J. Malakootikhah, *International Journal of Biological Macromolecules*, 2020, **153**, 421–432.
12 L. Hu, L. Chen, X. Peng, J. Zhang, X. Mo, Y. Liu and Z. Yan, *Microporous and Mesoporous Materials*, 2020, **299**, 110123.
13 Y. Dong and J. Zheng, *Chemical Engineering Journal*, 2020, **392**, 123690.
14 M. Ghahramaninezhad, F. Mohajer and M. Niknam Shahrak, *Front. Chem. Sci. Eng.*, 2020, **14**, 425–435.
15 S. Basu, A. Cano-Odena and I. F. J. Vankelecom, *Separation and Purification Technology*, 2011, **81**, 31–40.
16 V. Nafisi and M.-B. Hägg, *Journal of Membrane Science*, 2014, **459**, 244–255.
17 P. Z. Çulfaz, M. Wessling and R. G. H. Lammertink, *Journal of Membrane Science*, 2011, **369**, 221–227.
18 A. Huang, Y. Chen, N. Wang, Z. Hu, J. Jiang and J. Caro, *Chem. Commun.*, 2012, **48**, 10981.
19 M. Etxeberria-Benavides, O. David, T. Johnson, M. M. Łozińska, A. Orsi, P. A. Wright, S. Mastel, R. Hillenbrand, F. Kapteijn and J. Gascon, *Journal of Membrane Science*, 2018, **550**, 198–207.
20 F. Cacho-Bailo, M. Etxeberría-Benavides, O. Karvan, C. Téllez and J. Coronas, *CrystEngComm*, 2017, **19**, 1545–1554.
21 S. Aguado, J. Canivet and D. Farrusseng, *Chem. Commun.*, 2010, **46**, 7999.
22 H. Jin, Y. Li and W. Yang, *Ind. Eng. Chem. Res.*, 2018, **57**, 11963–11969.
23 S. Aguado, J. Canivet and D. Farrusseng, *J. Mater. Chem.*, 2011, **21**, 7582.
24 K. Martín-Betancor, S. Aguado, I. Rodea-Palomares, M. Tamayo-Belda, F. Leganés, R. Rosal and F. Fernández-Piñas, *Science of The Total Environment*, 2017, **595**, 547–555.
25 S. Aguado, J. Quirós, J. Canivet, D. Farrusseng, K. Boltes and R. Rosal, *Chemosphere*, 2014, **113**, 188–192.
26 W. Morris, N. He, K. G. Ray, P. Klonowski, H. Furukawa, I. N. Daniels, Y. A. Houndonougbo, M. Asta, O. M. Yaghi and B. B. Laird, *J. Phys. Chem. C*, 2012, **116**, 24084–24090.
27 A. M. Marti, M. Van and K. J. Balkus, *J Porous Mater*, 2014, **21**, 889–902.
28 R. J. Isaifan, S. Ntais and E. A. Baranova, *Applied Catalysis A: General*, 2013, **464–465**, 87–94.
29 A. Tavasoli, R. M. Kiai and A. Karimi, *Can. J. Chem. Eng.*, 2016, **94**, 1495–1503.

30 N. A. H. M. Nordin, A. F. Ismail, A. Mustafa, R. S. Murali and T. Matsuura, *RSC Adv.*, 2014, **4**, 52530–52541.
31 T. Johnson, M. M. Łozińska, A. F. Orsi, P. A. Wright, S. Hindocha and S. Poulston, *Green Chem.*, 2019, **21**, 5665–5670.
32 M. Gao, J. Wang, Z. Rong, Q. Shi and J. Dong, *RSC Adv.*, 2018, **8**, 39627–39634.
33 S. R. Venna, J. B. Jasinski and M. A. Carreon, *J. Am. Chem. Soc.*, 2010, **132**, 18030–18033.
34 M. C. McCarthy, V. Varela-Guerrero, G. V. Barnett and H.-K. Jeong, *Langmuir*, 2010, **26**, 14636–14641.
35 Mercury - The Cambridge Crystallographic Data Centre (CCDC), https://www.ccdc.cam.ac.uk/solutions/csd-system/components/mercury/, (accessed May 9, 2020).
36 Structures, https://www.ccdc.cam.ac.uk/structures/Search?Compound=ZIF-8&DatabaseToSearch=Published, (accessed May 9, 2020).
37 A. M. Aboraia, A. A. A. Darwish, V. Polyakov, E. Erofeeva, V. Butova, H. Y. Zahran, A. F. A. El-Rehim, H. Algarni, I. S. Yahia and A. V. Soldatov, *Optical Materials*, 2020, **100**, 109648.
38 A. Phan, C. J. Doonan, F. J. Uribe-Romo, C. B. Knobler, M. O'Keeffe and O. M. Yaghi, *Acc. Chem. Res.*, 2010, **43**, 58–67.
39 K. S. Park, Z. Ni, A. P. Cote, J. Y. Choi, R. Huang, F. J. Uribe-Romo, H. K. Chae, M. O'Keeffe and O. M. Yaghi, *Proceedings of the National Academy of Sciences*, 2006, **103**, 10186–10191.
40 M. Thommes, K. Kaneko, A. V. Neimark, J. P. Olivier, F. Rodriguez-Reinoso, J. Rouquerol and K. S. Sing, *Pure and Applied Chemistry*, 2015, **87**, 1051–1069.
41 M. Baias, A. Lesage, S. Aguado, J. Canivet, V. Moizan-Basle, N. Audebrand, D. Farrusseng and L. Emsley, *Angew. Chem. Int. Ed.*, 2015, **54**, 5971–5976.
42 P. Scherrer, in *Colloid chemistry a textbook*, Springer Berlin Heidelberg, 1912, pp. 387–409.
43 E. Shearier, P. Cheng, Z. Zhu, J. Bao, Y. H. Hu and F. Zhao, *RSC Adv.*, 2016, **6**, 4128–4135.
44 M. Jian, B. Liu, R. Liu, J. Qu, H. Wang and X. Zhang, *RSC Adv.*, 2015, **5**, 48433–48441.
45 H. Zhang, D. Liu, Y. Yao, B. Zhang and Y. S. Lin, *Journal of Membrane Science*, 2015, **485**, 103–111.